ISSN: (Print) (Online) Journal homepage: <https://www.tandfonline.com/loi/gcoo20>

Syntheses, structures and antimicrobial properties of complexes based on 2-hydroxybenzaldehyde-4-aminoantipyrine Schiff base

Quan Tang, Jing Hu, Yi-Jie Ding, Yi-Fan Zhang, Hui-Fang Li, Ming Xu, Xin-Cheng Yang, Lili Liang & Wen-Ge Li

To cite this article: Quan Tang, Jing Hu, Yi-Jie Ding, Yi-Fan Zhang, Hui-Fang Li, Ming Xu, Xin-Cheng Yang, Lili Liang & Wen-Ge Li (2021) Syntheses, structures and antimicrobial properties of complexes based on 2-hydroxybenzaldehyde-4-aminoantipyrine Schiff base, Journal of Coordination Chemistry, 74:4-6, 1039-1052, DOI: [10.1080/00958972.2021.1875449](https://doi.org/10.1080/00958972.2021.1875449)

To link to this article: <https://doi.org/10.1080/00958972.2021.1875449>



View supplementary material [↗](#)



Published online: 22 Jan 2021.



Submit your article to this journal [↗](#)



Article views: 49



View related articles [↗](#)



View Crossmark data [↗](#)



Syntheses, structures and antimicrobial properties of complexes based on 2-hydroxybenzaldehyde-4-aminoantipyrene Schiff base

Quan Tang, Jing Hu, Yi-Jie Ding, Yi-Fan Zhang, Hui-Fang Li, Ming Xu, Xin-Cheng Yang, Lili Liang  and Wen-Ge Li

Department of Chemistry, Bengbu Medical College, Bengbu, P. R. China

ABSTRACT

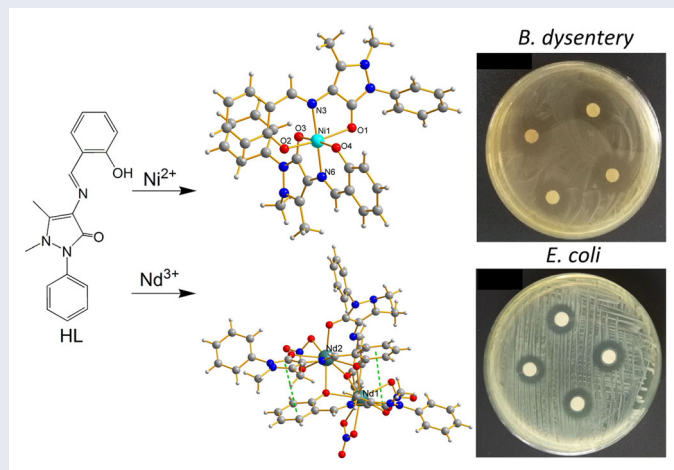
Two monomeric complexes, $[\text{NiL}_2 \cdot 3\text{H}_2\text{O}]$ (**1**) and $[\text{Nd}_2\text{L}_3(\text{NO}_3)_3]$ (**2**), with a tridentate ONO-donor Schiff base ligand HL (HL = 2-hydroxybenzaldehyde-4-aminoantipyrene) have been synthesized. Single-crystal X-ray diffraction analysis indicates that the asymmetric unit of **1** contains one Ni(II) and two L^- ligands, while **2** consists of two Nd(III) ions, three L^- ligands, and three NO_3^- ions. Complexes **1** and **2** are both 0-D discrete monomers, and there are intermolecular $\pi-\pi$ interactions in **1** and intramolecular $\pi-\pi$ interactions in **2**. The discrete $[\text{NiL}_2 \cdot 3\text{H}_2\text{O}]$ monomers are further connected through $\pi-\pi$ interactions, resulting in a 3-D supramolecular structure. Powder XRD and TG-DSC were performed for **1** and **2**. Antimicrobial experiments show that **1** displays significant antibacterial effect against *Bacillary dysentery* and *Escherichia coli* in comparison with that of Schiff base ligand.

ARTICLE HISTORY

Received 6 August 2020
Accepted 17 November 2020

KEYWORDS

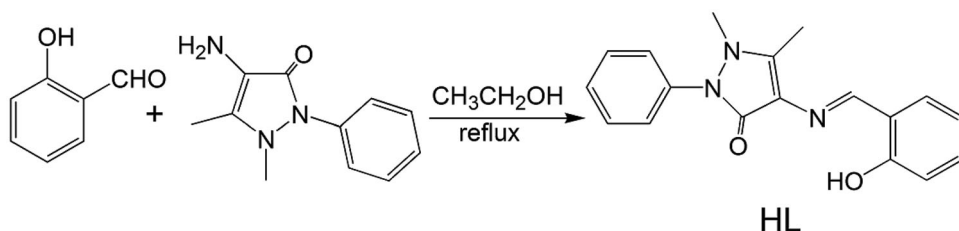
2-Hydroxybenzaldehyde;
4-aminoantipyrene; Schiff
base; antimicrobial activity



CONTACT Lili Liang  cll2162@163.com; Wen-Ge Li  lwg1010@163.com  Department of Chemistry, Bengbu Medical College, Bengbu 233030, P. R. China.

 Supplemental data for this article can be accessed <http://doi.org/10.1080/00958972.2021.1875449>.

© 2021 Informa UK Limited, trading as Taylor & Francis Group



Scheme 1. Synthetic route to Schiff base ligand HL.

1. Introduction

Coordination compounds have attracted considerable scientific interest as a kind of functional materials due to many applications, as well as their biological activities, such as antibacterial, antifungal, antiviral, anticancer [1–7]. Exploring new antibacterial materials such as imidazole derivatives [8, 9], Ag-based complexes [10, 11], Schiff base derivatives, and metal-based compounds have attracted attention [12–15]. Schiff base derivatives and metal-based complexes are the hottest research because Schiff base ligands with —N=CH— functional groups can coordinate with different metals to improve their antimicrobial activities [16–25]. Designing new materials with better antibacterial and anticancer activities is of immense importance in medicinal chemistry [26].

4-Aminoantipyrine derivatives are important biomodel compounds in biological systems for their potential biological, pharmacological, and medical applications [27, 28]. Exploring new bioactive compounds of 4-aminoantipyrine derivatives as antitumor, antibacterial, antiviral, or analgesic drugs is urgently needed. Furthermore, 4-aminoantipyrine derivatives were extensively used in coordination chemistry due to the coordination of keto- or aza-groups [29]. Schiff base and 4-aminoantipyrine derivatives are good candidates to explore new antibacterial materials. Herein, two monomeric complexes, $[\text{NiL}_2 \cdot 3\text{H}_2\text{O}]$ (**1**) and $[\text{Nd}_2\text{L}_3(\text{NO}_3)_3]$ (**2**), were constructed by a 4-aminoantipyrine Schiff base ligand, 2-hydroxybenzaldehyde-4-aminoantipyrine (abbreviated as HL, Scheme 1). The crystal structures of **1** and **2** together with HL were studied. PXRD, TG-DSC, and UV-Vis experiments and antimicrobial experiments were performed.

2. Experimental

2.1. Materials and instruments

All solvents and starting chemicals were purchased from commercial suppliers and used without purification. X-ray crystallographic data were collected on a Bruker Apex Smart APEX II X-ray single-crystal diffractometer. Elemental analyses for C, H, and N were carried out on a Perkin Elmer Series II CHNS/O 2400 element Analyzer. ^1H and ^{13}C NMR spectra of the ligand were recorded on a Bruker 400 MHz NMR. IR spectra were measured from a KBr pellet with a Nicolet iS50 FT-IR spectrometer from 4000 to 400 cm^{-1} . Thermal analyses were carried out with an STA 449-F5 analyzer with a heating rate of $5\text{ K}\cdot\text{min}^{-1}$. Powder X-ray diffraction (PXRD) patterns were collected in the 2θ range of 5° – 50° at a scan speed of $0.1^\circ\cdot\text{s}^{-1}$ on a Bruker D8 diffractometer at room

temperature in a nitrogen atmosphere. The UV-Vis spectra of HL, **1** and **2** were obtained on a Thermo Evolution 220 UV-Visible spectrophotometer. Conductivity measurements were performed on a Philips conductivity meter.

2.2. Synthesis of Schiff base ligand

An equimolar ethanol solution of 4-aminoantipyrine (0.4064 g, 2 mmol) and salicylaldehyde (0.2442 g, 2 mmol) was mixed and slightly heated (70 °C) for 6 h with stirring. The yellow resultant precipitate was filtered, washed several times with cold ethanol and then dried *in vacuo* over anhydrous CaCl₂ (Yield: 80%). The yellow precipitate was dissolved in methanol, and fine yellow crystals were obtained upon slow evaporation at room temperature. ¹H NMR (400 MHz, DMSO-d₆) δ: 12.98 (s, 1H), 9.71 (s, 1H), 7.55 (t, 2H), 7.47 (s, 2H), 7.40 (t, 3H), 7.32 (t, 1H), 6.92 (t, 2H), 3.21 (s, 3H), 2.40 (s, 3H). ¹³C NMR (100 MHz, DMSO-d₆) δ: 159.9, 159.5, 157.9, 150.7, 134.7, 132.2, 131.6, 129.7, 127.7, 125.4, 120.7, 119.7, 116.9, 114.5, 35.6, 10.3. IR (KBr pellet, cm⁻¹): 3424(w), 3062(w), 2936(w), 1606(s), 1655(s), 1592(s), 1456(m), 1348(m), 1269(m), 1153(m), 1139(m), 768(m), 730(w). Elemental analyses for C₁₈H₁₇N₃O₂ (%): C, 70.36; H, 5.54; N, 13.68. Found: C, 70.24; H, 5.48; N, 13.48.

2.3. Synthesis of [NiL₂·3H₂O] (1)

The nickel complex was synthesized by HL (0.03074 g, 0.1 mmol) and triethylamine (0.01 mL). The resulting mixture was added to ethanol solution of NiCl₂·6H₂O (0.02377 g, 0.1 mmol) and mixed. The reactants were transformed into 20 mL Teflon-sealed autoclave and subsequently heated to 85 °C for 72 h under autogenous pressure. After slowly cooling to room temperature, dark green crystals were formed. The crystals were isolated by filtration and washed with ethanol (Yield: 45%). IR (KBr pellet, cm⁻¹): 3852(w), 3750(w), 3648(w), 2360(s), 1606(s), 1533(s), 1435(s), 1395(m), 1331(m), 1202(m), 1153(m), 1042(m), 746(m), 734(w). Elemental analyses for C₃₆H₃₈N₆NiO₇ (%): C, 62.72; H, 5.28; N, 11.58. Found: C, 62.67; H, 5.34; N, 11.53.

2.4. Synthesis of [Nd₂L₃(NO₃)₃] (2)

The synthesis procedure of **2** is similar with **1** except using neodymium nitrate at 80 °C for 72 h (Yield: 65%). IR (KBr pellet, cm⁻¹): 3396(w), 1543(s), 1470(s), 1301(s), 1182(m), 1156(m), 1032(m), 843(m), 738(m), 715(w), 690(w). Elemental analyses for C₅₄H₄₈N₁₂Nd₂O₁₅ (%): C, 46.50; H, 3.44; N, 12.05. Found: C, 46.40; H, 3.32; N, 12.10.

2.5. Antimicrobial testing

Antimicrobial activities of the free ligand and the two complexes were tested *in vitro* by the disk diffusion method [30]. The test organisms were grown on nutrient agar media in petri plates. HL, **1** and **2** were prepared in DMSO (0.001 mol/L) and soaked in filter paper disks of 6 mm diameter and 0.3 mm thickness. The filter paper disks were placed on the previously seeded plates and incubated at 37 °C and after an incubation

period of 36 h at 37 °C, the diameters of inhibition area in mm were measured to evaluate antimicrobial activities of the compounds.

2.6. MIC experiment

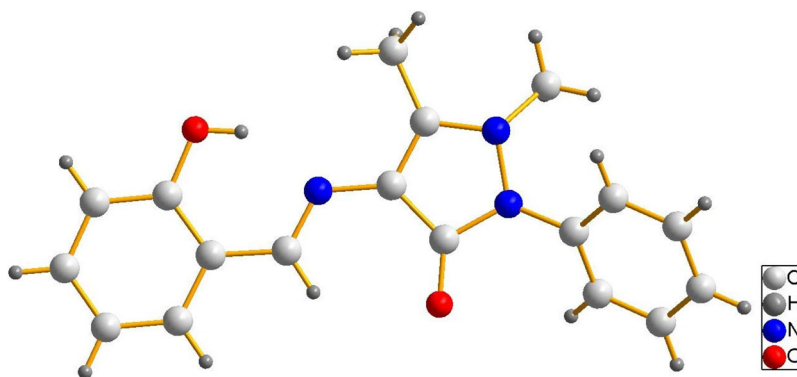
Minimum inhibitory concentrations (MICs) were evaluated using a broth microdilution method. The corresponding strains (*Bacillary Dysentery* or *Escherichia coli*) were seeded in culture medium and incubated at 37 °C for 20 h. It was subcultured and incubated in fresh culture medium for 20 h. The wells of a 96-well flat-bottomed microplate were filled with 100 μL of exponentially growing culture medium. Complex **1** and ciprofloxacin were dissolved in fresh culture medium with 1% DMSO, and the final solutions (1 mM, 100 μL) were added to the first well of each row and mixed evenly. The mixture solution of these wells (180 μL) was transferred to the second wells of each row. Similarly, a series of different concentration drug solutions (1 mM to 1.95 μM) was obtained in each row according to multiple dilution method. The last two wells of each row containing only the culture medium without diluted mixture solution were used as negative controls. The prepared strain solution (*B. Dysentery* or *E. coli*) (5 μL , 5×10^4 CFU/mL) was added to the wells of a 96-well microplate except the last wells of each row that were used as negative controls. The penultimate wells of each row were used as positive controls. The absorbance of each well was determined using an automatic ELISA tray reader adjusted at 620 nm [31]. The plate was incubated at 37 °C for 24 h, and the absorbance was read again in the reader at the same wavelength. These absorbance values were subtracted from those obtained before incubation. This procedure eliminated the interference of the tested substance. All tests were performed in triplicate. The MIC values for a drug were expressed as the lowest concentration that inhibits the bacterial growth.

2.7. X-ray crystallographic study

Suitable crystals were selected for single-crystal X-ray diffraction, and the data were collected on a Bruker Apex Smart APEX II X-Ray Single Crystal diffractometer with graphite-monochromated Mo-K α radiation ($\lambda = 0.71073 \text{ \AA}$) from an enhanced optic X-ray tube. Data reductions and absorption corrections were performed using the SAINT and SADABS software packages, respectively. The structure was solved by direct methods and refined by full-matrix least-squares methods on F^2 using SHELXS-97 and SHELXL-97, with atomic scattering factors for neutral atoms. Hydrogens were placed in calculated positions and refined as riding atoms with a uniform value of U_{iso} [32]. The guest solvent molecules in **1** are highly disordered and removed using PLATON squeeze refinement [33]. Elemental analyses and TGA data reveal that the chemical formula in **1** contains three water molecules. Selected crystal data and structural refinement parameters are summarized in Table 1. Selected bond lengths (\AA) and angles ($^\circ$) for **1** and **2** are summarized in supporting information Table S1.

Table 1. Crystallographic data for HL, 1 and 2.

Compound	HL	1	2
Formula	C ₁₈ H ₁₇ N ₃ O ₂	C ₃₆ H ₃₂ N ₆ NiO ₄	C ₅₄ H ₄₈ N ₁₂ Nd ₂ O ₁₅
Mr.	307.35	671.38	1393.52
Crystal system	Monoclinic	Monoclinic	Monoclinic
Space group	<i>P</i> ₂ (1)/ <i>n</i>	<i>P</i> ₂ (1)/ <i>n</i>	<i>P</i> ₂ (1)/ <i>n</i>
<i>Z</i>	4	4	4
<i>a</i> /Å	7.5418(12)	10.5012(15)	11.5683(5)
<i>b</i> /Å	7.4448(12)	13.453(2)	36.3925(15)
<i>c</i> /Å	27.102(4)	25.460(3)	12.7904(6)
α /°	90.00	90	90
β /°	95.402(7)	92.601(5)	94.358(2)
γ /°	90.00	90	90
Temperature /K	296	173	173
<i>V</i> /Å ³	1514.9(4)	3593.1(8)	5369.2(4)
<i>D</i> _c /g·cm ⁻³	1.348	1.241	1.724
μ /mm ⁻¹	0.090	0.585	1.995
<i>F</i> (000)	648	1400	2784
Crystal size/mm ³	0.26 × 0.17 × 0.08	0.18 × 0.15 × 0.12	0.09 × 0.08 × 0.05
Observed reflections	6529	15879	37876
Independent reflections	2554	6309	9467
Observed reflections (<i>I</i> > 2 σ (<i>I</i>))	1447	3503	6475
<i>R</i> _{int}	0.0705	0.1129	0.0987
GOF on <i>F</i> ²	1.046	1.041	1.046
<i>R</i> ₁ , <i>wR</i> ₂ [<i>I</i> > 2 σ (<i>I</i>)]	0.0673, 0.1385	0.0687, 0.1670	0.0561, 0.0820
<i>R</i> ₁ , <i>wR</i> ₂ [all data]	0.1431, 0.1749	0.0953, 0.1073	0.1060, 0.0938
CCDC No.	1972985	1936719	1935952

**Figure 1.** Molecular structure of HL.

3. Results and discussion

3.1. Crystal structure of the ligand

As depicted in Figure 1, the molecular structure of HL was confirmed by single X-ray diffraction analysis, which confirmed that the Schiff base was synthesized by condensation of 2-hydroxybenzaldehyde and 4-aminoantipyrine. In the free ligand, the phenolic ring is nearly coplanar with the pyrazole ring with a dihedral angle of 5.8(1)°, while the phenyl ring deviated a lot from the pyrazole ring with a dihedral angle of 43.3(1)°. There are π - π interactions between free ligands. As shown in Figure 2, the pyrazole ring of one L⁻ is parallel to the adjacent phenolic ring of the other free

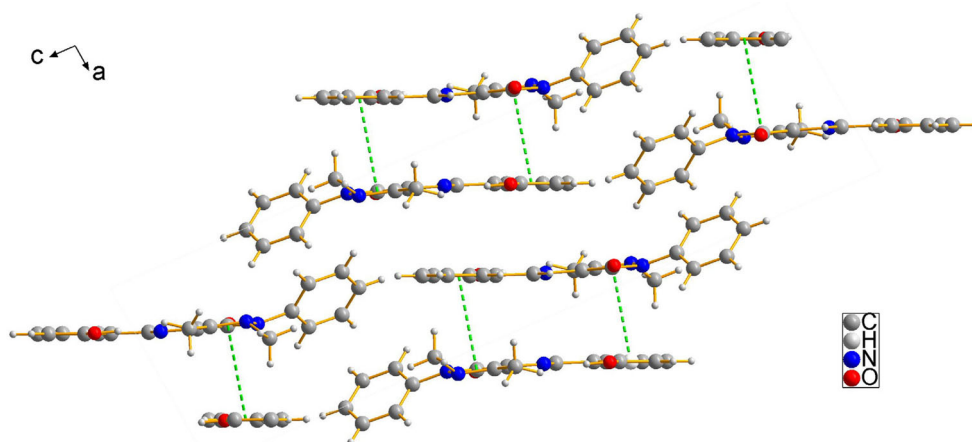


Figure 2. Two ligands are connected by π - π interactions (green-dotted lines).

ligand with the dihedral angle of 0° and the centroid-to-centroid distance of 3.8852(5) Å. So every two ligands are further connected by π - π interactions.

3.2. ^1H NMR spectra of the ligand

The ^1H NMR spectra of the ligand were obtained in DMSO-d_6 using TMS as an internal standard. The free ligand has a sharp singlet at 12.98 ppm, which is due to hydrogen-bonded phenolic protons. The sharp singlet at 9.71 ppm is from the $\text{CH}=\text{N}$ proton. The nine protons of four triplets and one doublet within the range 6.92–7.55 ppm should be the two aromatic ring protons. The signals for the two $-\text{CH}_3$ groups were observed at 3.21 (N- CH_3) and 2.40 ppm, respectively.

3.3. Crystal structure of **1**

X-ray crystallographic analysis reveals that **1** crystallizes in monoclinic space group $P_2(1)/n$. The asymmetric unit contains one Ni(II) and two unique L^- ligands. As shown in Figure 3, the central Ni(II) in **1** lies nearly in the twofold rotation axis, coordinated with two tridentate L^- ligands. Each ligand provides two O atoms (one hydroxy and one carbonyl) and one N atom forming five- and six-membered chelating rings. Ni(II) has a slightly distorted octahedral geometry by four oxygen and two nitrogen atoms. The four oxygens (O(1), O(2), O(3), and O(4)) and Ni(1) are nearly coplanar with two nitrogens on both sides. The bond lengths [Ni-N = 2.029(5), 2.045(5) and Ni-O of 1.989(4) to 2.184(4) Å] around Ni(II) ions are within normal ranges. The two L^- ligands have similar configurations in **1**, different than free ligand. The pyrazole ring of one ligand has a dihedral angle of $46.9(2)^\circ$ with the phenyl ring and an angle of $15.6(2)^\circ$ with the phenolic ring, while the pyrazole ring of the other ligand has a dihedral angle of $52.6(2)^\circ$ and $12.0(2)^\circ$, respectively.

There are intermolecular π - π interactions in **1**. The pyrazole ring of one L^- is nearly parallel to the adjacent phenolic ring of the other L^- with dihedral angle of $15.6(2)^\circ$ and centroid-to-centroid distance of 3.7257(4) Å; the other L^- ligand has dihedral angle of $17.8(2)^\circ$ and centroid-to-centroid distance of 3.8146 Å. Every phenolic ring in

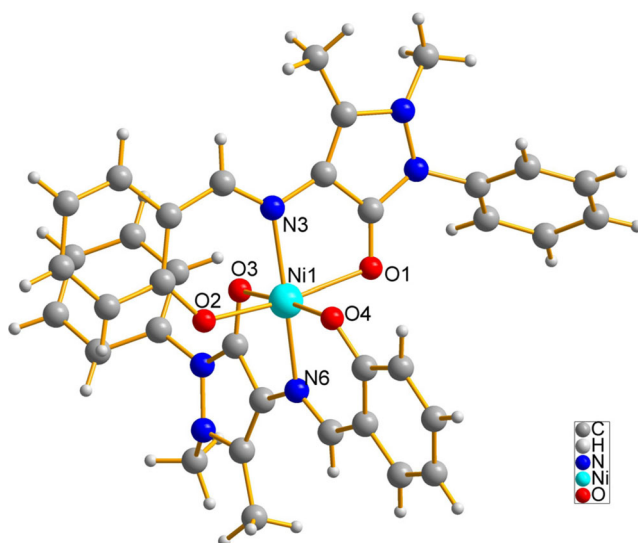


Figure 3. Molecular structure of **1**.

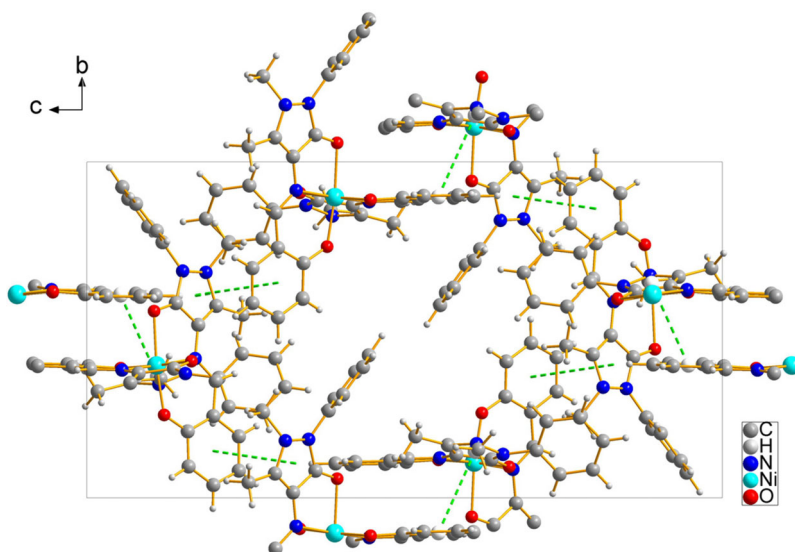


Figure 4. Packing diagram of **1** showing four individual π - π interactions (green-dotted lines).

1 is further connected to adjacent pyrazole ring of the other L^- ligand, so **1** is further connected through four individual π - π interactions (Figure 4). Thus, the 0-D discrete $[\text{NiL}_2]$ monomers are further connected through π - π interactions, resulting in a 3-D supramolecular structure.

3.4. Crystal structure of **2**

Complex **2** crystallizes in the monoclinic space group $P_2(1)/n$. Its asymmetric unit consists of two Nd(III) ions, three L^- ligands, and three NO_3^- ions. As depicted in Figure 5, Nd₁ is

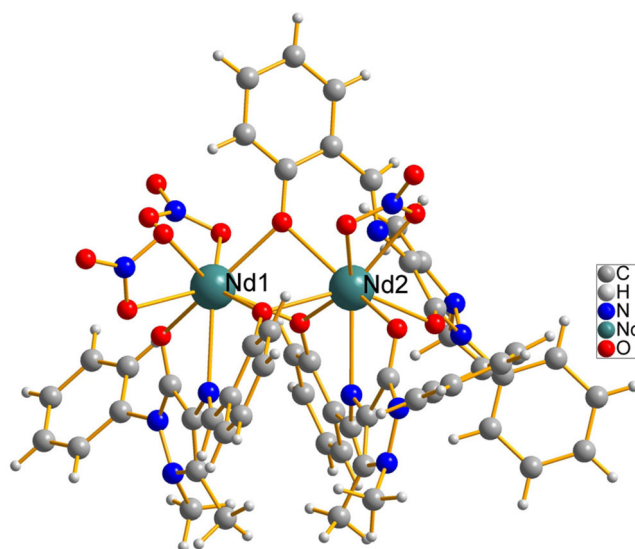


Figure 5. Molecular structure of **2**.

nine-coordinate with one nitrogen from one L^- , four oxygen atoms from two NO_3^- ions and four oxygens from three L^- ligands, two oxygens from hydroxy and carbonyl of one L^- ligand, and two oxygens from two hydroxy groups of two L^- ligands. Nd_2 is also nine-coordinate by two nitrogens from two L^- ligands, two oxygens from one NO_3^- ion, and five oxygens from three L^- ligands in a distorted polyhedral geometry, in which four oxygens from two hydroxy and carbonyl groups of two L^- ligands. The coordination environment of Nd_2 and Nd_1 ions is different. Nd_1 and Nd_2 are further bridged by three μ_2-O atoms from hydroxy of three L^- ligands to form a $[Nd_2(\mu_2-O)_3]$ dimer. Each ligand provides two O atoms (one μ_1-O from carbonyl, one μ_2-O from hydroxy) and one N-forming five- and six-membered chelating rings. The three L^- ligands in **2** have different configurations. Two L^- ligands are similar configurations with dihedral angles between pyrazole ring and phenolic ring of $57.4(2)^\circ$ and phenyl ring of $32.9(2)^\circ$ in one ligand. The dihedral angle between pyrazole ring and phenolic ring is $46.3(2)^\circ$ and phenyl ring of $34.4(2)^\circ$ in the other ligand. The third L^- is very different with angles between pyrazole ring and phenolic ring, phenyl ring of $70.3(2)^\circ$ and $54.2(2)^\circ$, respectively.

There are two individual $\pi-\pi$ stacking interactions within **2**. As shown in [Figure 6](#), the pyrazole ring of one L^- (connecting Nd_2) is nearly parallel to the phenolic ring of the other L^- ligand with dihedral angle of $15.7(2)^\circ$ and centroid-to-centroid distance of $3.5397(1)$ Å. At the same time, the pyrazole ring of one L^- (connecting Nd_1) is nearly parallel to the phenolic ring of the other L^- ligand with dihedral angle of $17.3(3)^\circ$ and centroid-to-centroid distance of $3.6287(1)$ Å. So the two L^- ligands are further connected by intramolecular $\pi-\pi$ stacking interactions.

3.5. Conductance measurements

The molar conductivities of **1** and **2** in DMSO (1 mM) were measured at room temperature. The molar conductance of the free ligand, **1** and **2** is 2, 10, and

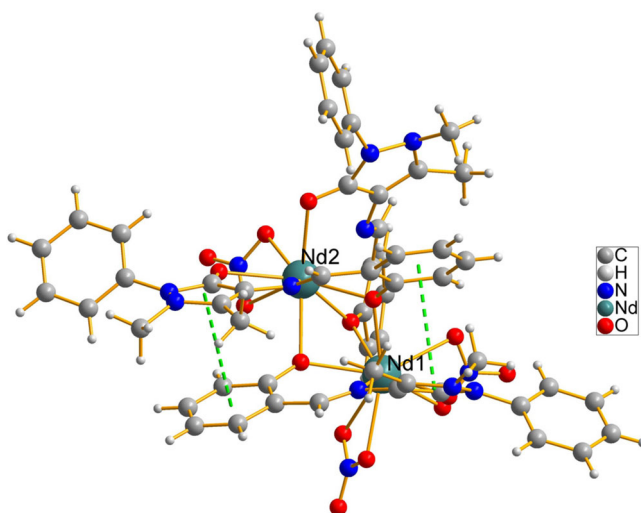


Figure 6. Two individual π - π interactions within **2** (green-dotted lines show the π - π interaction).

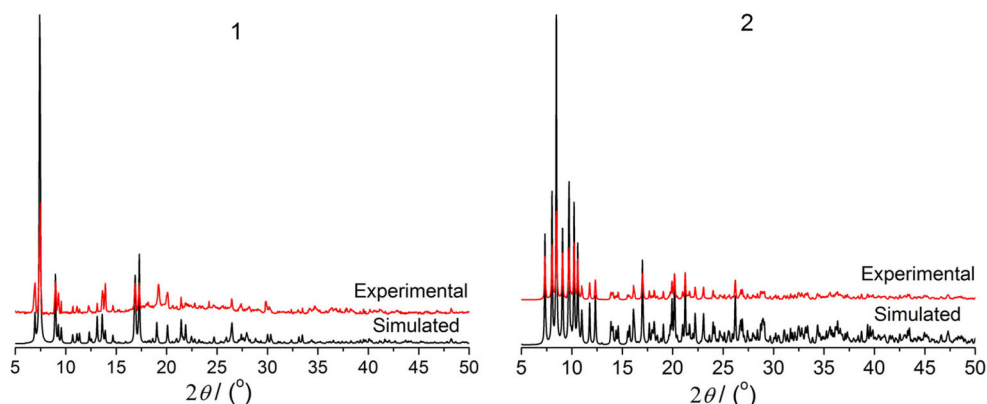


Figure 7. Powder XRD patterns of **1** and **2**.

$11 \text{ ohm}^{-1} \text{ mol}^{-1} \text{ cm}^2$, respectively. It is concluded from the results that the free ligand and **1** and **2** have low molar conductance values, indicating non-electrolytic nature of the free ligand and two complexes, so there are no anions present outside the coordination sphere.

3.6. Powder X-ray patterns and thermalgravimetric analyses

PXRD experiments were carried out to check the phase purity and homogeneity of **1** and **2**. As presented in Figure 7, the main peak positions of the experimental patterns match well with the simulated ones from their single-crystal X-ray structures using Mercury 3.0 software, indicating consistency with bulk samples. Pyrolysis behaviors of **1** and **2** were also investigated with thermal gravimetric analysis (TGA) and differential scanning calorimetry (DSC). TGA analysis (Figure 8) reveals that **1** has two weight loss steps. The first of 7.34% at 150°C with a small endothermic peak corresponds to the

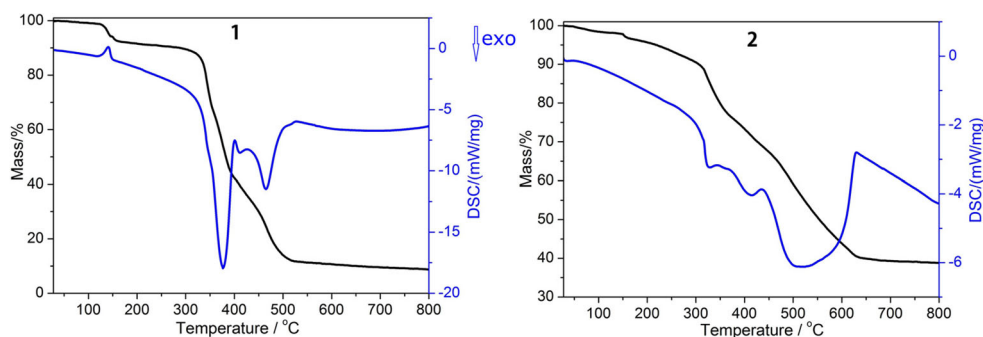


Figure 8. TG-DSC curves of **1** and **2**.

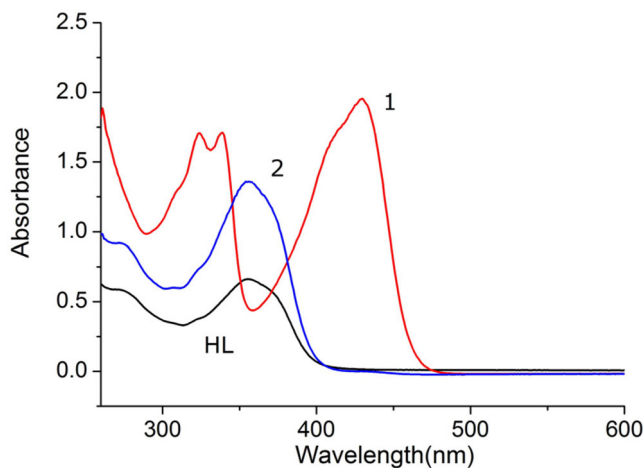


Figure 9. UV-Vis spectra of the free ligand, **1** and **2** in DMSO solution.

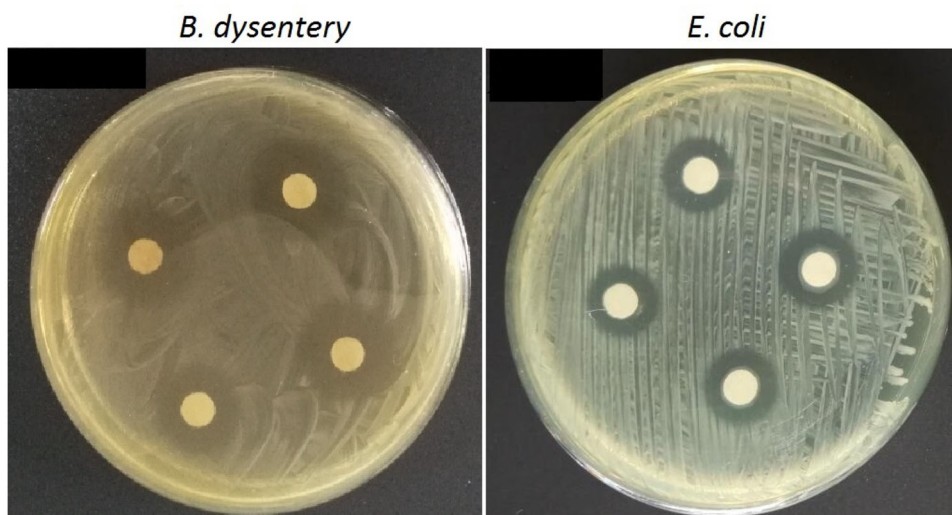
loss of three guest water molecules (calcd 7.44%). The framework decomposed sharply at 350 °C with a big exothermic peak. The residual species were assumed to be NiO above 500 °C (obsd. 10.36%, calcd 10.30%). For **2**, the first gradual weight loss of 9.0% from 50 – 300 °C corresponds to the loss of two coordinated NO₃[−] ions (calcd 8.9%), which is followed closely with the collapse of the whole framework at 300 – 630 °C. The residue above 700 °C should be an equimolar mixture of neodymium carbonate and neodymium nitrate (obsd. 38.8%, calcd 38.21%).

3.7. UV-Vis absorption spectra

UV-Vis absorption spectra of the free ligand, **1** and **2** were recorded in DMSO solution from 260–600 nm at room temperature (Figure 9). The ligand displays moderate intensity absorption at 355 nm from the π - π^* transition of the C=N bonds in aromatic rings. Compound **2** has similar absorption bands with that of the free ligand with stronger intensity. For **1**, the first double absorption peaks at 324 and 338 nm should be due to the intraligand charge transfer transitions. The strong absorption peak at 430 nm is typical for octahedrally coordinated Ni(II) complexes [34]. The extinction

Table 2. Antibacterial results of **1**, **2**, HL and ciprofloxacin by inhibition zone diameter (mm).

Tested material	<i>B. dysentery</i>	<i>E. coli</i>	<i>S. aureus</i>	<i>C. albicans</i>
1	22	12	—	—
2	—	—	8	—
HL	—	—	—	—
Ciprofloxacin	26	12	27	—

**Figure 10.** Images of inhibition zones for **1** against *B. dysentery* and *E. coli*.

coefficients of the free ligand, **1** and **2** are 6.6×10^2 , 1.36×10^3 , and 1.96×10^3 $\text{L} \cdot \text{mol}^{-1} \cdot \text{cm}^{-1}$, respectively.

3.8. Antimicrobial studies

Antimicrobial properties of the free ligand, **1** and **2** in DMSO were assessed by evaluating their activity using the disk diffusion method. Gram-positive bacteria *Staphylococcus aureus*, Gram-negative bacteria *Bacillary dysentery* and *E. coli*, and fungal *Candida albicans* were selected to evaluate the antimicrobial activities [35]. Ciprofloxacin was chosen as the positive control drug. Four parallel experiments were performed, and the average diameters are listed in Table 2. As shown in Figure 10, the average diameter of inhibition zone reaches 22 mm, which shows significant inhibition of **1** against *B. dysentery*, but is still lower than the positive control drug ciprofloxacin of 30 mm. The average inhibition zone diameter of **1** against *E. coli* was 12 mm, which means moderate inhibition, whereas no inhibition effect towards Gram-positive bacteria *S. aureus* of **1** could be observed, nor antifungal activity against *C. albicans* under identical experimental conditions. The results showed that **1** has antibacterial activities against Gram-negative bacteria *B. dysentery* and *E. coli*. The antimicrobial results show that **2** has limited inhibition effect against *S. aureus* with average diameter of 8 mm, while no inhibition effect toward *B. dysentery*, *E. coli*, and *C. albicans*. The antimicrobial results show the inhibition effects of the ligand towards

S. aureus, *B. dysentery*, *E. coli*, and *C. albicans* are small under identical experimental conditions, indicating that the Schiff base does not have significant antimicrobial activity.

The MIC determined by the spectrophotometric method was defined as the concentration at which there was a sharp decline in the absorbance value (supporting information Figure S3). For **1**, MIC values of *B. dysentery* and *E. coli* are 500 and 1000 μM , respectively, higher than the positive control drug ciprofloxacin (125 and 250 μM). The MIC values of **1** are consistent with the results of previous antibacterial experiments. Complex **1** showed moderate antibacterial activity against *B. dysentery* and relatively weak antibacterial activity against *E. coli*. Although antibacterial activities of **1** against both strains are weaker than that of ciprofloxacin, these findings are significant to the design of antibacterial compounds. New Schiff base complexes with 4-aminoantipyrine derivatives can be obtained by introducing different types of substituents into the benzene ring, which may enhance the antibacterial activity of these complexes. Further research is in progress.

On comparing biological activity of the Schiff base and its metal complexes, the antibacterial activity follows the order of **1** > **2** > L. Neither the free ligand nor the two complexes showed inhibition on *Candida*. One possible reason is that the transition metal ions are drug carriers making the complex have better distribution coefficient of lipid and water [36]. As a result, the complex could reach the target site through the biofilm easier and enhanced its efficacy. Another possible reason is that the increase in antibacterial activity of **1** may be due to the presence of metal ions coordinated with the donor atoms of the Schiff base ligand, rearranging into a distorted octahedral geometry which might affect normal cell processes, such as cellular uptake, protein, and/or DNA biosyntheses [37, 38]. As a rare earth metal ion, Nd(III) usually possesses certain antibacterial activity; however, **2** does not show antibacterial activity, which is possibly caused by the unique molecular structure of the complex. It is important to study the relationship between the structure of Schiff base complex and the antibacterial activity in order to define the mechanism of pharmacological activities.

4. Conclusion

Complexes **1** and **2** were synthesized with a tridentate 4-aminoantipyrine-derived Schiff base ligand HL and characterized by single-crystal X-ray diffraction. They both have discrete monomer structures, and there are π - π interactions between monomer **1** and within monomer **2**. Monomer **1** is further connected through π - π interactions, resulting in a 3-D supramolecular structure. HL has configurations in **1** and **2** different than that of free ligand. The antimicrobial results showed **1** has significant antibacterial effect against *B. dysentery* and *E. coli* in comparison with that of Schiff base ligand. We expect that this synthetic strategy may open a new way to fabrication of complexes based on 4-aminoantipyrine Schiff bases as antibacterial materials.

Disclosure statement

No potential conflict of interest was reported by the authors.

Funding

This work was financially supported by Natural Science Foundation of Bengbu Medical University [Grant BYTM2019001, BYKY1701ZD], 512 Talent Cultivation Foundation [by51201201], Anhui Province Natural Science Foundation [1908085MB45], and National University Student Innovation and Entrepreneurship Training Project [Grant 201710367031]

ORCID

Lili Liang  <http://orcid.org/0000-0003-1594-5253>

References

- [1] G.M. Espallargas, E. Coronado. *Chem. Soc. Rev.*, **47**, 533 (2018).
- [2] L. Wang, J. Li, L. Zhang, Y. Fang, C. Chen, Y. Zhao, Y. Song, L. Deng, G. Tan, X. Wang, P.P. Power. *J. Am. Chem. Soc.*, **139**, 17723 (2017).
- [3] J.F. Katherine, M.-N. Nils. *Chem. Rev.*, **119**, 727 (2019).
- [4] L.E. Kreno, K. Leong, O.K. Farha, M. Allendorf, R.P. Van Duyne, J.T. Hupp. *Chem. Rev.*, **112**, 1105 (2012).
- [5] L.J. Zhou, W.H. Deng, Y.L. Wang, G. Xu, S.G. Yin, Q.Y. Liu. *Inorg. Chem.*, **55**, 6271 (2016).
- [6] J. Della Rocca, D. Liu, W. Lin. *Acc. Chem. Res.*, **44**, 957 (2011).
- [7] G. Chen, B. Yu, C. Lu, H. Zhang, Y. Shen, H. Cong. *CrystEngComm*, **20**, 7486 (2018).
- [8] D. Mantu, V. Antoci, C. Moldoveanu, G. Zbancioc, I.I. Mangalagiu. *J. Enzyme Inhib. Med. Chem.*, **31**, 96 (2016).
- [9] L. Liang, M. Miao, C. Liu, Z. Zong, J. Zhang, Q. Fang. *New J. Chem.*, **43**, 16691 (2019).
- [10] Y. Jiang, C.F. Zhu, Z. Zheng, J.B. He, Y. Wang. *Inorg. Chim. Acta*, **451**, 143 (2016).
- [11] A.Z. El-Sonbati, M.A. Diab, A.A. El-Bindary, M.I. Abou-Dobara, H.A. Seyam. *Spectrochim. Acta A Mol. Biomol. Spectrosc.*, **104**, 213 (2013).
- [12] G.G. Mohamed, M.M. Omar, A.A. Ibrahim. *Eur. J. Med. Chem.*, **44**, 4801 (2009).
- [13] M. Manimohan, S. Pugalmani, M.A. Sithique. *Int. J. Biol. Macromol.*, **136**, 738 (2019).
- [14] Y. Chen, P. Li, S. Su, M. Chen, J. He, L. Liu, M. He, H. Wang, W. Xue. *RSC Adv.*, **9**, 23045 (2019).
- [15] N. Venugopal, G. Krishnamurthy, H.S. Bhojyanaik, M. Giridhar. *J. Mol. Struct.*, **1191**, 85 (2019).
- [16] F. Zhao, W. Wang, W. Lu, L. Xu, S. Yang, X.-M. Cai, M. Zhou, M. Lei, M. Ma, H.-J. Xu, F. Cao. *Eur. J. Med. Chem.*, **146**, 451 (2018).
- [17] Z. Mou, N. Deng, F. Zhang, J. Zhang, J. Cen, X. Zhang. *Eur. J. Med. Chem.*, **138**, 72 (2017).
- [18] C.L. Zhang, X.Y. Qiu, S.-J. Liu. *J. Coord. Chem.*, **72**, 3248 (2019).
- [19] X. Liu, J.R. Hamon. *Coord. Chem. Rev.*, **389**, 94 (2019).
- [20] Y. Xu, Y. Shi, F. Lei, L. Dai. *Carbohydr. Polym.*, **230**, 115671 (2020).
- [21] R. Fekri, M. Salehi, A. Asadi, M. Kubicki. *Inorg. Chim. Acta*, **484**, 245 (2019).
- [22] Y.-X. Sun, W.-X. Wei, Q.-L. Hao, L.-D. Lu, X. Wang. *Spectrochim. Acta A Mol. Biomol. Spectrosc.*, **73**, 772 (2009).
- [23] M.R. Hasan, M.A. Hossain, M.A. Salam, M.N. Uddin. *J. Taibah University Sci.*, **10**, 766 (2016).
- [24] M.N. Uddin, S. Khandaker, Moniruzzaman, M.S. Amin, W. Shumi, M.A. Rahman, S.M. Rahman. *J. Mol. Struct.*, **1166**, 79 (2018).
- [25] D.A. Chowdhury, M.N. Uddin, F. Hoque. *Chiang Mai J. Sci.*, **37**, 443 (2010).
- [26] K. Mahmood, W. Hashmi, H. Ismail, B. Mirza, B. Twamley, Z. Akhter, I. Rozas, R.J. Baker. *Polyhedron*, **157**, 326 (2019).
- [27] J. Joseph, K. Nagashri, G.A.B. Rani. *J. Saudi Chem. Soc.*, **17**, 285 (2013).
- [28] P.A. Fatullayeva, A.A. Medjidov, A.M. Maharramov, A.V. Gurbanov, R.K. Askerov, K.Q. Rahimov, M.N. Kopylovich, K.T. Mahmudov, A.J.L. Pombeiro. *Polyhedron*, **44**, 72 (2012).

- [29] P. Sen, T. Nyokong. *Polyhedron*, **173**, 114135 (2019).
- [30] M.N. Uddin, D.A. Chowdhury, K. Hossain. *J. Chin. Chem. Soc.*, **59**, 1520 (2012).
- [31] K.F. Devienne, M.S.G. Raddi. *Braz. J. Microbiol.*, **33**, 166 (2002).
- [32] G.M. Sheldrick. SHELXS-97, Program for the Solution of Crystal Structures, University of Göttingen, Germany (1997).
- [33] A.L. Spek. *PLATON*, the University of Utrecht, Utrecht (1999).
- [34] L. Qin, J.S. Hu, Y.Z. Li, H.G. Zheng. *Cryst. Growth Des.*, **12**, 403 (2012).
- [35] M.B. Halli, R.B. Sumathi. *Arabian J. Chem.*, **10**, S1748 (2017).
- [36] E. Yousif, A. Majeed, K. Al-Sammarrae, N. Salih, J. Salimon, B. Abdullah. *Arabian J. Chem.*, **10**, S1639 (2017).
- [37] N.D. Al-Khathami, K.S. Al-Rashdi, B.A. Babgi, M.A. Hussien, M. Nadeem Arshad, N.E. Eltayeb, S.E. Elsilik, J. Lasri, A.S. Basaleh, M. Al-Jahdali. *J. Saudi Chem. Soc.*, **23**, 903 (2019).
- [38] Y. Gou, J. Li, B. Fan, B. Xu, M. Zhou, F. Yang. *Eur. J. Med. Chem.*, **134**, 207 (2017).